environmental microbiology

Environmental Microbiology (2020) **22**(12), 5090–5108 doi:10.1111/1462-2920.15094

The ROK-family regulator Rok7B7 directly controls carbon catabolite repression, antibiotic biosynthesis, and morphological development in *Streptomyces avermitilis*

Xiaorui Lu,[1] Xingchao Liu,[1] Zhi Chen,[1] Jilun Li,[1] Gilles P. van Wezel,[2] Wei Chen[3*] and Ying Wen[1*]

[1]*State Key Laboratory of Agrobiotechnology and College of Biological Sciences, China Agricultural University, Beijing, China.*

[2]*Molecular Biotechnology, Institute of Biology, Leiden University, Leiden, The Netherlands.*

[3]*Clinical Research Center, the Second Hospital of Nanjing, Nanjing University of Chinese Medicine, Nanjing, China.*

Summary

Carbon catabolite repression (CCR) is a common phenomenon in bacteria that modulates expression of genes involved in uptake of alternative carbon sources. In the filamentous streptomycetes, which produce half of all known antibiotics, the precise mechanism of CCR is yet unknown. We report here that the ROK-family regulator Rok7B7 pleiotropically controls xylose and glucose uptake, CCR, development, as well as production of the macrolide antibiotics avermectin and oligomycin A in *Streptomyces avermitilis*. Rok7B7 directly repressed structural genes for avermectin biosynthesis, whereas it activated *olmRI*, the cluster-situated activator gene for oligomycin A biosynthesis. Rok7B7 also directly repressed the xylose uptake operon *xylFGH*, whose expression was induced by xylose and repressed by glucose. Both xylose and glucose served as Rok7B7 ligands. *rok7B7* deletion led to enhancement and reduction of avermectin and oligomycin A production, respectively, relieved CCR of *xylFGH*, and increased co-uptake efficiency of xylose and glucose. A consensus Rok7B7-binding site, 5′-TTKAMKHSTTSAV-3′, was identified within *aveA1p*, *olmRIp*, and *xylFp*, which allowed prediction of the Rok7B7 regulon and confirmation of 11 additional targets involved in development, secondary metabolism, glucose uptake, and primary metabolic processes. Our findings will facilitate methods for strain improvement, antibiotic overproduction, and co-uptake of xylose and glucose in *Streptomyces* species.

Received 8 February, 2020; revised 10 May, 2020; accepted 19 May, 2020. *For correspondence. E-mail njyy039@njucm.edu.cn; Tel. (+86) 25 85091648. E-mail wen@cau.edu.cn; Tel. (+86) 10 62732715. [Correction added on 03 July 2020 after first online publication: The affiliation of the 5th and 6th author has been corrected in this version.]

Introduction

The Gram-positive bacterial streptomycetes is known for two unique traits: (i) production of a wide variety of medically useful antibiotics and (ii) a complex life cycle involving the successive formation of vegetative hyphae, aerial hyphae, and chains of spores (Flardh and Buttner, 2009; van Wezel and McDowall, 2011). Carbon catabolite repression (CCR), a process occurring in streptomycetes and other bacteria that ensures the preferred uptake of carbon source (e.g., glucose) despite the presence of alternative ones in the environment. CCR also plays a role in the control of development and antibiotic production in streptomycetes where glucose is usually the driver of this process (van Wezel and McDowall, 2011; Romero-Rodriguez *et al*., 2017). In streptomycetes, glucose is transported through the major facilitator superfamily (MFS) transporter GlcP and phosphorylated by glucose kinase (GlkA) and not through the phosphoenolpyruvate-dependent phosphotransferase system (PTS) (van Wezel *et al*., 2005). GlkA plays a role in CCR (van Wezel and McDowall, 2011; Romero-Rodriguez *et al*., 2017) even if it lacks a DNA-binding domain. The way GlkA exerts its regulatory role is unknown. In summary, our knowledge regarding regulation of CCR in streptomycetes at the molecular level is very poor, despite many decades of research.

At least 20 families of transcriptional regulators (TRs) have been discovered in streptomycetes, including TetR, LuxR, MarR, AraC, LysR, GntR, SARP, and ROK (Repressor, Open Reading Frame, Kinase) (Romero-Rodriguez *et al*., 2015). The ROK-family regulators have

a characteristic PF00480 motif and are widely distributed in prokaryotes, but the specificity and function for most of them remain unknown (Kazanov *et al*., 2013). ROK-family regulators characterized so far are involved mainly in sugar metabolism; e.g., Mlc and NagC in *E. coli* regulate uptake of glucose and N-acetylglucosamine (GlcNAc) respectively (Plumbridge, 2001). The best-studied ROK-family regulator in streptomycetes is *S. lividans* CsnR that auto-regulates negatively its own expression as well as that of a chitosanase encoding gene in response to products of chitosan degradation (Dubeau *et al*., 2011). In *S. coelicolor*, Rok7B7 (SCO6008) is involved in the control of antibiotic production, development, xylose uptake, and CCR (Swiatek *et al*., 2013), but its specific DNA-binding sites and ligands have not been identified. In this strain, another ROK-family regulator, RokB (SCO6115) acts as a direct regulator of heterologously expressed novobiocin biosynthetic gene cluster (BGC). The predicted RokB regulon suggests involvement of RokB in transport and metabolism of amino acids, but not of sugars (Bekiesch *et al*., 2016). Furthermore, the effect of deletion of genes encoding other ROK-family regulators, SCO0794, SCO1060, SCO2846, SCO7543, SCO6566, or SCO6600 on the development and antibiotic production of *S. coelicolor* was reported (Swiatek *et al*., 2013). Therefore, the manipulation of regulatory networks governed by ROK-family regulators might be beneficial for strain improvement and thus deserves deeper investigation.

The industrially important species *S. avermitilis* is a well-known producer of avermectins, which are economically potent anthelmintic antibiotics widely applied in agricultural and medical fields (Burg *et al*., 1979; Egerton *et al*., 1979). *Streptomyces avermitilis* also produces oligomycin A, a 26-membered macrolide antibiotic that displays antifungal and antitumor activities (Pinna *et al*., 1967; Lin *et al*., 2009). The 82-kb avermectin BGC contains one cluster-situated regulator (CSR) gene, *aveR*, that encodes a LuxR-family activator essential for expression of *ave* structural genes (Guo *et al*., 2010; Kitani *et al*., 2009). The ~100-kb oligomycin BGC contains two CSR genes, *olmRI* and *olmRII*, that encode LuxR-family activators essential for oligomycin biosynthesis (Yu *et al*., 2012). The *S. avermitilis* genome encodes 17 putative ROK-family regulators (including Rok7B7 orthologue SAV_2248), of which none has been studied so far.

In the present study, we characterized *S. avermitilis* Rok7B7 as a dual repressor/activator in development, avermectin and oligomycin A production, xylose and glucose uptake, and other primary metabolic processes. Rok7B7 targets associated with these processes were identified. Both xylose and glucose act as ligands of Rok7B7 and its orthologues from model *S. coelicolor* and *S. venezuelae*, but they play opposing roles in modulating its DNA-binding activity. Repression of the xylose uptake operon *xylFGH* by glucose-induced CCR is dependent on Rok7B7. We also described a novel strategy for increasing avermectin yield and improving co-uptake efficiency of xylose and glucose through deletion of *rok7B7* gene.

Results

Rok7B7 affects development and biosynthesis of avermectins and oligomycin A

The gene *rok7B7* (*sav_2248*) from *S. avermitilis* consists of 1200 nucleotides (nt) and encodes a 399-amino acid protein. Protein alignment showed a high conservation, with 91.2%, 90%, 94%, 94.3% and 94.3% overall amino acid identity to its orthologs in *S. griseus*, *S. venezuelae*, *S. scabies*, *S. lividans*, and *S. coelicolor* respectively. *rok7B7* is located upstream of the *xylFGH* operon (*sav_2247*, *sav_2246*, *sav_2245*) that encodes a xylose ABC transport system (Swiatek *et al*., 2013) and is transcribed in the same direction as the latter (Fig. 1). *xylG* overlaps *xylH* with 4 bp, and the intergenic regions *xylF-xylG* and *rok7B7-xylF* are 184 and 123 bp long respectively (Fig. 1). RT-PCR analysis revealed that *xylF* is co-transcribed with *xylG*, whereas *rok7B7* is not co-transcribed with *xylF* (Supporting Information Fig. S1), indicating that *xylF*, *xylG*, and *xylH* form an operon and *rok7B7* has its own promoter.

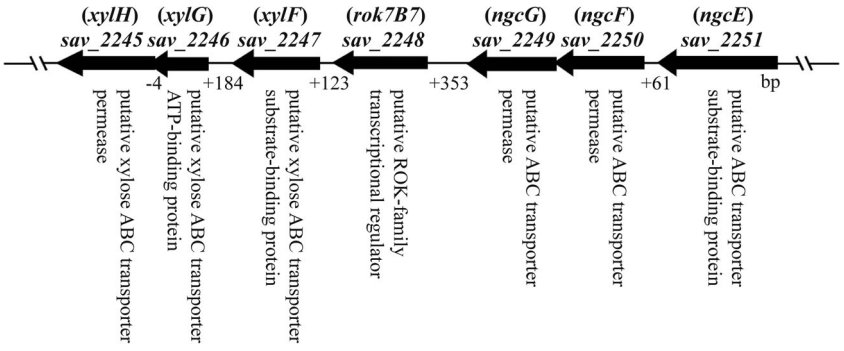

Fig. 1. Genetic organization of *rok7B7* and its neighbouring genes.

To investigate the role of Rok7B7 in *S. avermitilis*, we constructed a mutant strain with an in-frame deletion of *rok7B7* (Δrok7B7) (Supporting Information Fig. S2), this mutant complemented with a single copy of *rok7B7* (Crok7B7) and a strain, which overexpresses *rok7B7* (Orok7B7). qRT-PCR analyses revealed that *rok7B7* transcription was undetectable in Δrok7B7, and that its level in Orok7B7 was ∼1.6-fold higher on day 2 (exponential phase) and ∼5.4-fold higher on day 6 (stationary phase) than that in the wild-type (WT) strain (Supporting Information Fig. S3), confirming deletion or overexpression of *rok7B7* in the strains.

Δrok7B7, Crok7B7, and Orok7B7 were grown on solid YMS sporulation medium for phenotypic comparison with WT. Δrok7B7 displayed earlier differentiation and sporulation, whereas Orok7B7 and Crok7B7 were similar to WT (Fig. 2A). Faster differentiation of Δrok7B7 was confirmed by scanning electron microscopy (SEM) of samples grown on YMS plates for 2 or 4 days (Fig. 2B). On day 2, WT colonies mainly consisted of vegetative mycelia, whereas Δrok7B7 colonies were already sporulated. On day 4, both strains formed spore chains. These findings indicate an inhibitory role of Rok7B7 in *S. avermitilis* development.

We then investigated the effects of deletion and overexpression of *rok7B7* on growth and antibiotic biosynthesis. Quantitative analysis by HPLC of the fermentation broth from 10-day cultures grown in FM-I showed that, relative to WT level, avermectin yield was increased by ∼106% in Δrok7B7, but was reduced by ∼46% in Orok7B7. Avermectin production of the complemented mutant Crok7B7 and of control strains (WT/pKC1139, WT/pSET152) was nearly identical to that of WT (Fig. 3A). Oligomycin A yield was reduced by ∼38% in Δrok7B7 and increased by ∼78% in Orok7B7 relative to WT level (Fig. 3B). Biomass accumulation of Δrok7B7 and Orok7B7 grown in soluble FM-II was similar to that of WT (Fig. 3C), indicating that altered antibiotic yields of Δrok7B7 and Orok7B7 were not due to changes of cell growth. These findings indicate that Rok7B7 differentially regulates production of avermectins and oligomycin A.

In view of the significant increase of avermectin yield resulting from the deletion of *rok7B7*, we also deleted the gene in industrial strain 63#, using the same strategy as for WT, and examined the effect on avermectin yield. In shake-flasks, avermectin yield was ∼13%–16% higher for Δrok7B7/63# than for 63# (Fig. 3D). Although in this case, the deletion of *rok7B7* does not seem to have had much effect in the industrial strain, compared with the WT, it is a potentially efficient strategy to enhance avermectin production in industrial strains.

Rok7B7 represses avermectin structural genes and activates the gene for oligomycin CSR

Transcription of *rok7B7* in WT grown in FM-I was assessed by qRT-PCR to further establish the role of Rok7B7 in the control of antibiotic production in *S. avermitilis*. *rok7B7* transcript levels reached a maximum after 2 days of growth, followed by a gradual decrease, reaching low levels after 6 days (Fig. 4A). Simultaneously, Rok7B7 protein levels were examined by western blotting. Expression of fusion protein Rok7B7-3FLAG in Δrok7B7 (strain Δrok7B7/rok7B7-3FLAG) restored avermectin production

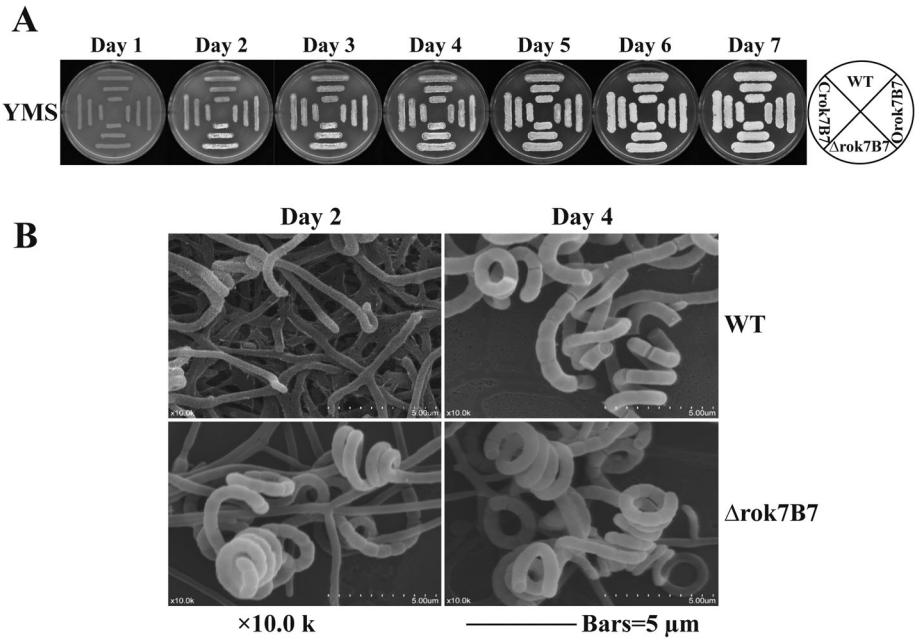

Fig. 2. Effect of Rok7B7 on *S. avermitilis* development.
A. Phenotypes of WT strain, *rok7B7* deletion mutant (Δrok7B7), complemented strain (Crok7B7), and overexpression strain (Orok7B7) grown on YMS plates at 28°C.
B. SEM images of WT and Δrok7B7 after growth on YMS plates for 2 or 4 days.

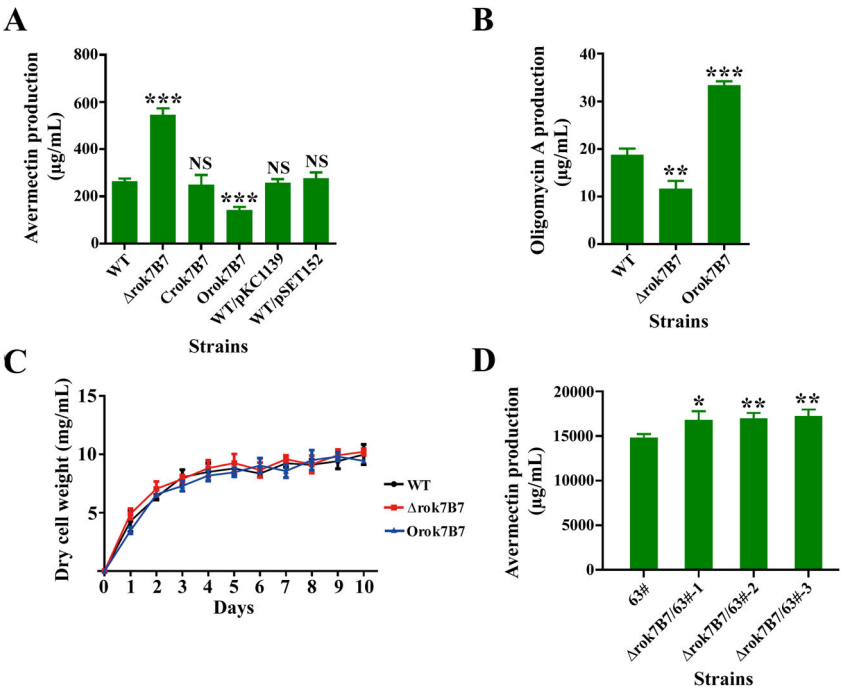

Fig. 3. Effects of Rok7B7 on antibiotic production and cell growth in *S. avermitilis*.
A and B. Yield of avermectins (A) and oligomycin A (B) in *rok7B7*-related strains cultured in FM-I for 10 days. WT/pSET152 and WT/pKC1139 are the empty vector control strains.
C. Growth curves of WT, Δrok7B7, and Orok7B7 cultured in FM-II.
D. Avermectin yield in industrial strain 63# and its derivatives Δrok7B7/63#-1, -2, and -3 (*rok7B7* deletion strains) grown in FM-I for 10 days. Error bars (all panels): SD from triplicate experiments. Statistical notations (panels A, B, D): NS, not significant; $^{*}P < 0.05$; $^{**}P < 0.01$; $^{***}P < 0.001$ for comparison with WT (A, B) or 63# (D) (Student's *t*-test). [Color figure can be viewed at wileyonlinelibrary.com]

to WT level (Supporting Information Fig. S4), indicating that Rok7B7-3FLAG complemented Rok7B7 function, and that Rok7B7 expression profile could be monitored with anti-FLAG antibody against Rok7B7-3FLAG in Δrok7B7/rok7B7-3FLAG. Consistent with the transcriptional profile, Rok7B7 protein level was maximal after 2 days, low after 6 days and barely detectable from day 7 onward (Fig. 4B). These findings indicate that Rok7B7 plays its role particularly toward the end of exponential phase.

To determine whether Rok7B7 regulates avermectin and oligomycin A production directly through CSR genes or structural genes, we performed electrophoretic mobility shift assays (EMSAs) using soluble His_6-tagged Rok7B7 purified from *E. coli*. Probes corresponding to the promoter regions of three CSR genes, namely *aveRp*, *olmRIp*, and *olmRIIp*, were used for EMSAs (Fig. 4C). The *ave* gene cluster contains four genes for polyketide synthase (PKS), namely *aveA1*, *aveA2*, *aveA3*, and *aveA4*, which synthesize the avermectin polyketide backbone. *aveA1* and *aveA2* are co-transcribed, and *aveA4* and *aveA3* are co-transcribed (Ikeda *et al*., 1999). The seven PKS genes in the *olm* gene cluster form two transcriptional units: *olmA1-olmA2-olmA3-olmA6-olmA7* and *olmA4-olmA5* (Omura *et al*., 2001). Accordingly, we designed promoter probes *aveA1p* (for *aveA1-aveA2*), *aveA4p* (for *aveA4-aveA3*), *olmA1p* (for *olmA1-olmA2-olmA3-olmA6-olmA7*), and *olmA4p* (for *olmA4-olmA5*) for EMSA probes of structural genes (Fig. 4C). As control we used the probe *hrdBp*, corresponding to the promoter region of *hrdB*, which encodes the principal RNA polymerase σ factor HrdB. His_6-Rok7B7 bound specifically to probes *aveA1p* and *olmRIp*, but not to *aveRp*, *aveA4p*, *olmRIIp*, *olmA1p*, or *olmA4p*, nor to the negative control *hrdBp* (Fig. 4D). Binding specificities were confirmed by competition assays using ~300-fold unlabeled specific probes (lanes S) or non-specific probe *hrdBp* (lanes N). *aveA2* is co-transcribed with *aveA1*, and is therefore also a target of Rok7B7.

To confirm *in vivo* binding of Rok7B7 to target promoters of *aveA1* and *olmRI*, we performed chromatin immunoprecipitation-quantitative PCR (ChIP-qPCR) assays using samples from WT and Δrok7B7/rok7B7-3FLAG cultured in soluble FM-II for 1–6 days, and anti-FLAG mAb against Rok7B7-3FLAG. WT without Rok7B7-3FLAG was used as negative control. *aveRp* did not display Rok7B7 enrichment (Fig. 4E), confirming that *aveR* is indirectly regulated by Rok7B7. In contrast, Rok7B7 bound to *aveA1p* and *olmRIp* at various time points; binding was strongest at day 2 and decreased thereafter (Fig. 4E), consistent with the expression profile of Rok7B7. These findings confirm dynamic binding of Rok7B7 to the target promoters *aveA1p* and *olmRIp in vivo*.

The effect of Rok7B7 on the expression of target genes *aveA1*, *aveA2*, and *olmRI* was assessed by qRT-PCR. RNA samples were isolated after 2 and 6 days from WT and Δrok7B7 grown in FM-I. *aveA1* and *aveA2* transcription levels were higher in Δrok7B7 at both time points, whereas *olmRI* level in Δrok7B7 was lower, consistent with the antibiotic yield data for Δrok7B7 (Fig. 4F).

These experiments revealed an interesting difference in the avermectin and oligomycin A production

controlled by Rok7B7: Rok7B7 interacted with the promoter regions of the *ave* structural genes but not with that of the activator gene *aveR*, while, in contrast, Rok7B7 interacted with the promoter region of the activator gene of oligomycin biosynthetic cluster.

Determination of Rok7B7-binding sites

Understanding the regulatory mechanism of Rok7B7 on its target promoters requires determination of precise Rok7B7-binding sites. Despite many such efforts using DNase I footprinting assays, we were unable to detect

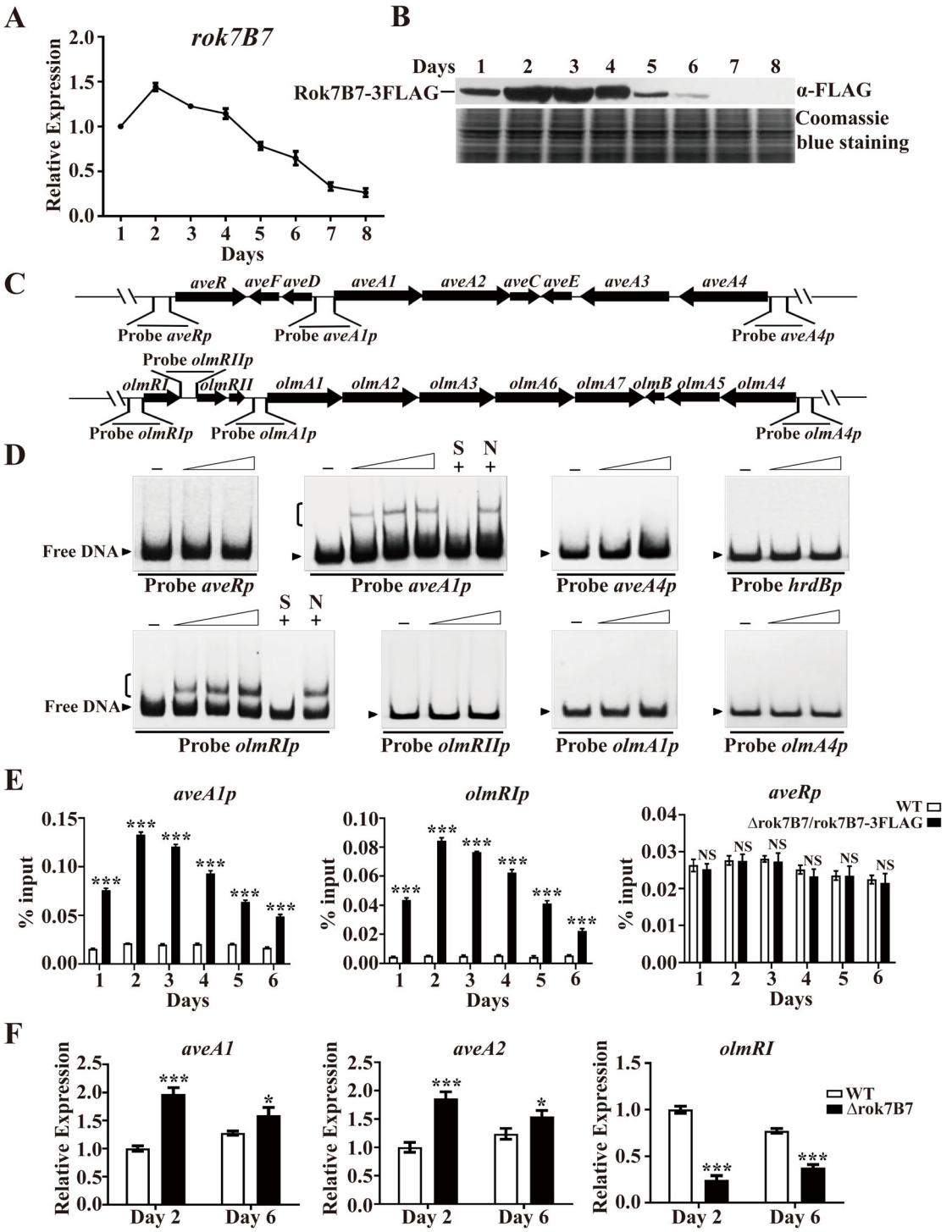

Fig. 4. Legend on next page.

Rok7B7-binding sites on promoter regions of any of the identified target genes, most likely because of the low DNA-binding activity of Rok7B7. We therefore performed EMSAs, using a series of overlapping probes, to identify the protected site of Rok7B7 on *aveA1p*. Overlapping probes *aveA1p*-I and *aveA1p*-II covered the entire 303-bp *aveA1p* probe, and a 108-bp overlapping sequence was designated as probe *aveA1p*-III (Fig. 5A). His_6-Rok7B7 bound to probes *aveA1p*-I, *aveA1p*-II, and *aveA1p*-III (Fig. 5A), indicating that the Rok7B7-binding site(s) on *aveA1p* are located within the 108-bp overlapping region.

DNAMAN analysis of the 108-bp sequence of probe *aveA1p*-III revealed a direct repeat sequence (**TTGAA**GAG**TTGAA**; termed DR^{ave}) and a palindromic sequence (**TTGAA**GACG**TTCAA**; termed IR^{ave}). To shorten the Rok7B7 binding region, we designed a 50-bp probe *aveA1p*-IV containing both sequences DR^{ave} and IR^{ave}. EMSAs of His_6-Rok7B7/probe *aveA1p*-IV interaction revealed a band shift, suggesting that DR^{ave} or IR^{ave} may serve as target site for Rok7B7 binding. To evaluate relative contributions of DR^{ave} and IR^{ave} in Rok7B7 binding, we introduced mutations into repeat motifs of probe *aveA1p*-IV to generate a series of 50-bp mutated probes (Fig. 5B). His_6-Rok7B7 bound to probe 3 m but not to 1 m, 2 m, or 4 m (Fig. 5B), indicating that the 5-bp direct repeats in sequence DR^{ave}, but not inverted repeats in IR^{ave}, are essential for Rok7B7 binding.

As TRs typically bind to similar DNA motifs in target promoter regions, we searched and found an imperfect direct repeat sequence (**TTGAC**TCG**TTCAG**; termed DR^{olm}) similar to DR^{ave} in probe *olmRIp*. The ability of Rok7B7 to bind to DR^{olm} was evaluated by EMSAs using 50-bp probes containing either intact sequence DR^{olm} (termed probe *olmRIp*-I) or the mutated sequence lacking direct repeats (termed probe 5 m) (Fig. 5C). Affinity of His_6-Rok7B7 for the mutated probe 5 m was abolished in comparison with corresponding WT probe *olmRIp*-I (Fig. 5C), indicating that the direct repeats in DR^{olm} play an essential role in Rok7B7 binding.

Binding kinetics of Rok7B7 with 50-bp probes *aveA1p*-IV and *olmRIp*-I, respectively containing Rok7B7-binding sites DR^{ave} and DR^{olm}, were studied by biolayer interferometry (BLI) assay. The sensorgrams revealed a direct correlation of binding strength with His_6-Rok7B7 concentration. The equilibrium dissociation constants (K_D) for interaction with Rok7B7 were 31.7 and 13.9 nM for *aveA1p*-IV and for *olmRIp*-I, respectively (Fig. 5D). Thus, DNA affinity of Rok7B7 was much lower than that of CsnR, the ROK-family regulator from *S. lividans* (K_D values of CsnR were respectively 0.032 and 0.040 nM for *csnA* and *csnR* operators) (Dubeau *et al*., 2011).

The role of Rok7B7 in the transcriptional control of *aveA1* and *olmRI* was further examined using 5′ rapid amplification of cDNA ends (5′ RACE) to identify promoter structures of the two genes (Supporting Information Fig. S5). The *aveA1* TSS was localized to a G located 137 nt upstream of the *aveA1* translational start codon (TSC) (Fig. 5E), and the *olmRI* TSS was mapped to a G located 138 nt upstream of the *olmRI* TSC (Fig. 5E). Rok7B7-binding site DR^{ave} on *aveA1* promoter region extends from positions −7 to +6 relative to *aveA1* TSS and is close to the putative −10 region (Fig. 5E). Binding of repressor close to −10 sequence is common. It is likely that Rok7B7 inhibits *aveA1* transcription by hindering recruitment of RNA polymerase. Rok7B7-binding site DR^{olm} on *olmRI* promoter region extends from positions −12 to +1 relative to *olmRI* TSS and overlaps the putative −10 region (Fig. 5E). Binding of transcriptional activator to −10 sequence is unusual; however, the binding site of master developmental repressor BldD in the *eryB*VI promoter region overlaps the −10 sequence, and BldD positively regulates erythromycin production (Chng *et al*., 2008). Analogously, the SARP (*Streptomyces* antibiotic regulatory protein)-family regulators, *e.g*., AfsR (Tanaka *et al*., 2007), FdmR1 (Chen *et al*., 2008), and OtcR (Yin *et al*., 2015), interact with direct repeats close to the −10 regions and presumably activate transcription of target genes by recruiting RNA polymerase to the promoters. The regulatory mechanism of transcriptional activation in the present case remains to be elucidated.

FIG. 4. Rok7B7 directly regulates *aveA1* and *olmRI*.

A. Transcriptional profile of *rok7B7* in WT grown in FM-I. Transcription level of *rok7B7* on day 1 was defined as 1.

B. Western blotting analysis of Rok7B7 protein level during fermentation process. Rok7B7 temporal expression in strain Δrok7B7/rok7B7-3FLAG grown in FM-I was analysed using anti-FLAG mAb. Loading control: Coomassie blue staining of 80 μg total protein loaded per lane.

C. Schematic representation of promoter probes for EMSAs.

D. EMSAs of interactions of His_6-Rok7B7 with the indicated promoter probes. Negative probe: *hrdBp*. Each lane contained 0.3 nM labelled probe. Concentrations of His_6-Rok7B7 for probes *aveA1p* and *olmRIp*: 250, 500, and 750 nM; for other probes: 500 and 750 nM; 750 nM His_6-Rok7B7 was used for competition assays (lanes +). Lanes −: EMSAs without His_6-Rok7B7. Lanes N and S: competition experiments with ~300-fold excess of unlabelled nonspecific probe *hrdBp* (N) and specific probe (S). Arrow: free probe. Bracket: Rok7B7-DNA complex.

E. ChIP-qPCR assays of Rok7B7 binding to *aveA1p*, *olmRIp*, and *aveRp*. Anti-FLAG mAb against Rok7B7-3FLAG was used to immunoprecipitate Rok7B7-3FLAG-DNA complexes from 1, 2, 3, 4, 5, and 6 days cultures of Δrok7B7/rok7B7-3FLAG treated with formaldehyde. WT strain was used as negative control. Y-axis: relative value of Rok7B7 enrichment on each site, determined by comparison of qPCR cycle number for ChIP sample with that for input DNA.

F. qRT-PCR analysis of *aveA1*, *aveA2*, and *olmRI* in WT and Δrok7B7 grown in FM-I. Transcription level was calculated relative to WT level on day 2, defined as 1. Error bars (panels A, E, F): SD from triplicate experiments. Statistical notations (panels E, F): NS, not significant; $*P < 0.05$; $***P < 0.001$ for comparison with WT (*t*-test). [Color figure can be viewed at wileyonlinelibrary.com]

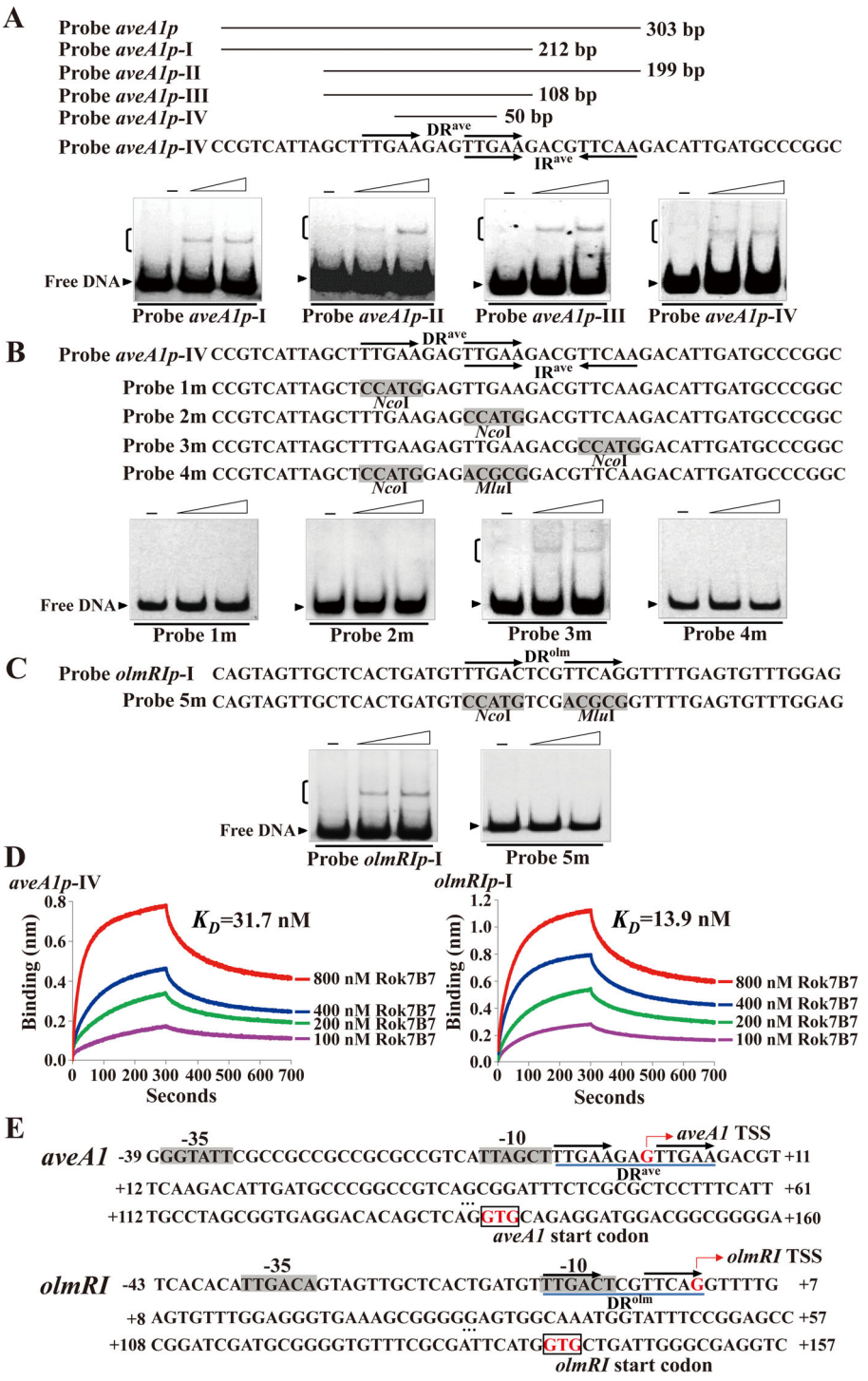

Fig. 5. Rok7B7-binding sites on promoter regions of *aveA1* and *olmRI*.
A. EMSAs of His_6-Rok7B7 with probes located within *aveA1* promoter region. Relative probe positions and lengths are shown schematically. Straight arrows: inverted or direct repeats. Lanes 2 and 3: 500 and 750 nM His_6-Rok7B7.
B. EMSAs using mutated 50-bp probes of *aveA1p*-IV. Mutations were introduced into inverted or direct repeats of WT probe *aveA1p*-IV to produce mutated probes 1 m, 2 m, 3 m, and 4 m. Shading: altered nucleotides.
C. EMSAs using 50-bp WT probe *olmRIp*-I and its mutated probe 5 m. Direct repeats in probe *olmRIp*-I were replaced with *Nco*I and *Mlu*I sites to produce mutated probe 5 m.
D. Interaction kinetics of Rok7B7 with probes *aveA1p*-IV and *olmRIp*-I determined by BLI analysis. Biotin-labelled DNA probe (300 nM) was loaded on streptavidin sensor and interacted with His_6-Rok7B7 at concentrations 100, 200, 400, and 800 nM.
E. Nucleotide sequences of *aveA1* and *olmRI* promoter regions and Rok7B7-binding sites. Numbers: distance (nt) from respective TSS. Red bent arrows: TSSs. Shading: presumed –10 and –35 regions. Boxes: TSCs. Underlining: Rok7B7-binding sites. Straight arrows: direct repeats. [Color figure can be viewed at wileyonlinelibrary.com]

Rok7B7 affects xylose and glucose uptake

ROK-family regulators are generally associated with sugar metabolism, and *S. coelicolor* Rok7B7 was shown to affect xylose and glucose uptake (Swiatek *et al*., 2013). We therefore investigated the role of *S. avermitilis* Rok7B7 in control of sugar uptake. Growth of WT, Δrok7B7, and Orok7B7 was assessed in liquid MM cultures containing xylose, glucose, maltose, or mannitol as sole carbon source. With xylose or glucose as carbon source, growth rate and biomass yield were higher for Δrok7B7 and lower for Orok7B7 than for WT (Fig. 6A). Consistent with biomass yield, WT consumed 39% of xylose and 36% of

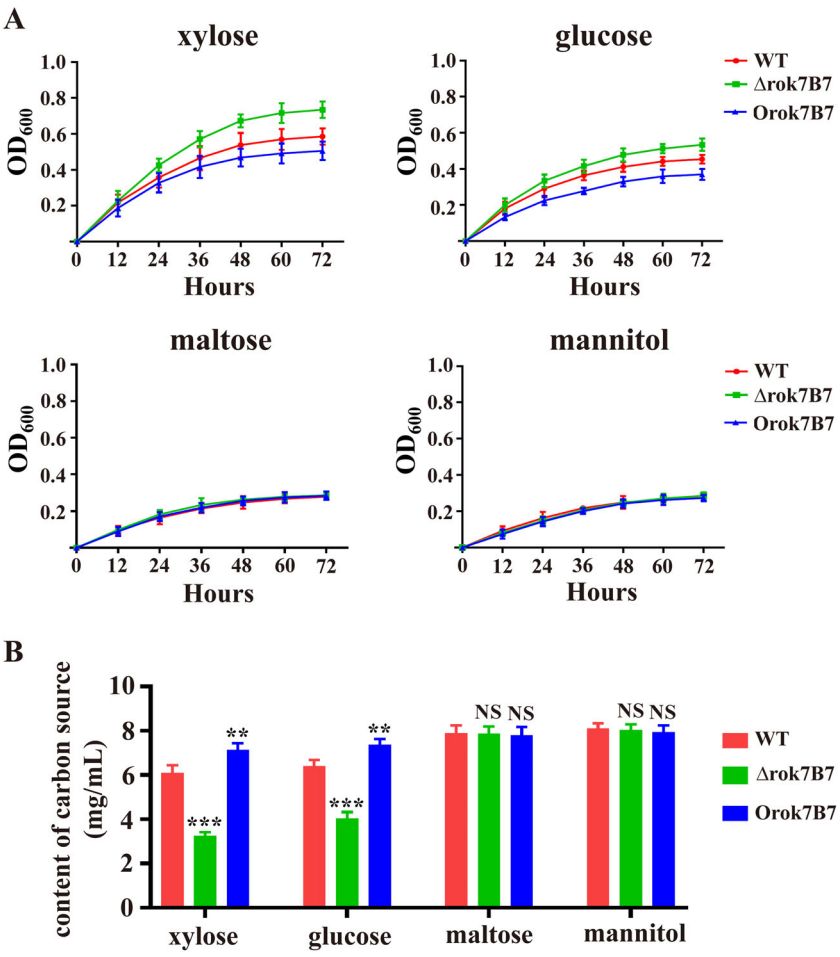

Fig. 6. Effects of Rok7B7 on xylose and glucose uptake.
A. Growth curves of WT, Δrok7B7, and Orok7B7 in liquid MM with various carbon sources (10 mg mL^{-1}). Biomass is expressed as OD_{600} (optical density at wavelength 600 nm).
B. Content of carbon sources remaining in liquid MM after 72 h culture of the above strains. Error bars: SD from triplicate experiments. NS, not significant; $^{**}P < 0.01$; $^{***}P < 0.001$ for comparison with WT (*t*-test). [Color figure can be viewed at wileyonlinelibrary.com]

glucose, respectively, after 72 h culture, while Δrok7B7 consumed 67% of xylose and 59% of glucose, and Orok7B7 consumed 29% of xylose and 25% of glucose (Fig. 6B). With maltose or mannitol as carbon source, growth rate and biomass yield did not differ appreciably among the three strains (Fig. 6A). Consumption of maltose and mannitol by the three strains was similar, i.e., ~20% for maltose and ~19% for mannitol (Fig. 6B). These findings indicate that Rok7B7 represses xylose and glucose uptake in *S. avermitilis*.

Rok7B7 directly represses the xylFGH operon

The xylose transport operon *xylFGH* is adjacent to *rok7B7*, and 5-bp direct repeats (**TTTAC**TTC**TTGAC**; termed DR^{xyl}) similar to those in sequence DR^{ave} are present in promoter region of *xylF*. To test if Rok7B7 regulates the *xylFGH* operon, EMSAs were performed using probe *xylFp* that contains the *xylFGH* promoter region. Indeed, His_6-Rok7B7 was able to interact with probe *xylFp*, whereas His_6-Rok7B7 did not auto-regulate its own transcription (probe *rok7B7p*) (Fig. 7A). Direct binding of Rok7B7 to *xylFp* but not to *rok7B7p* was confirmed *in vivo* by ChIP-qPCR assays (Fig. 7B).

The role of sequence DR^{xyl} in Rok7B7 binding was examined by performing site-directed mutagenesis of 50-bp WT probe *xylFp*-I (containing intact DR^{xyl}) on the direct repeats to generate mutated probe 6 m, which lacked direct repeats (Fig. 7C). Binding of Rok7B7 to WT probe *xylFp*-I and to 6 m was evaluated by EMSAs. His_6-Rok7B7 bound to *xylFp*-I but not to 6 m (Fig. 7C), indicating that the direct repeats in DR^{xyl} are essential for Rok7B7 binding.

BLI assays revealed a K_D of Rok7B7/*xylFp*-I interaction of 47.5 nM (Fig. 7D), which is lower than for *aveA1p*-IV (K_D = 31.7 nM) or *olmRIp*-I (K_D = 13.9 nM). qRT-PCR analysis showed that transcript levels of *xylF*, *xylG* and *xylH* were higher for Δrok7B7 than for WT grown in FM-I (Fig. 7E), and thus that Rok7B7 represses the operon.

Most *Streptomyces* strains contain another *xyl* gene locus, *xylABR*, involved in xylose uptake. XylA (xylose isomerase) catalyses isomerization of xylose to xylulose, and XylB (xylulose kinase) mediates phosphorylation of xylulose to xylulose-5-phosphate. XylR acts as a

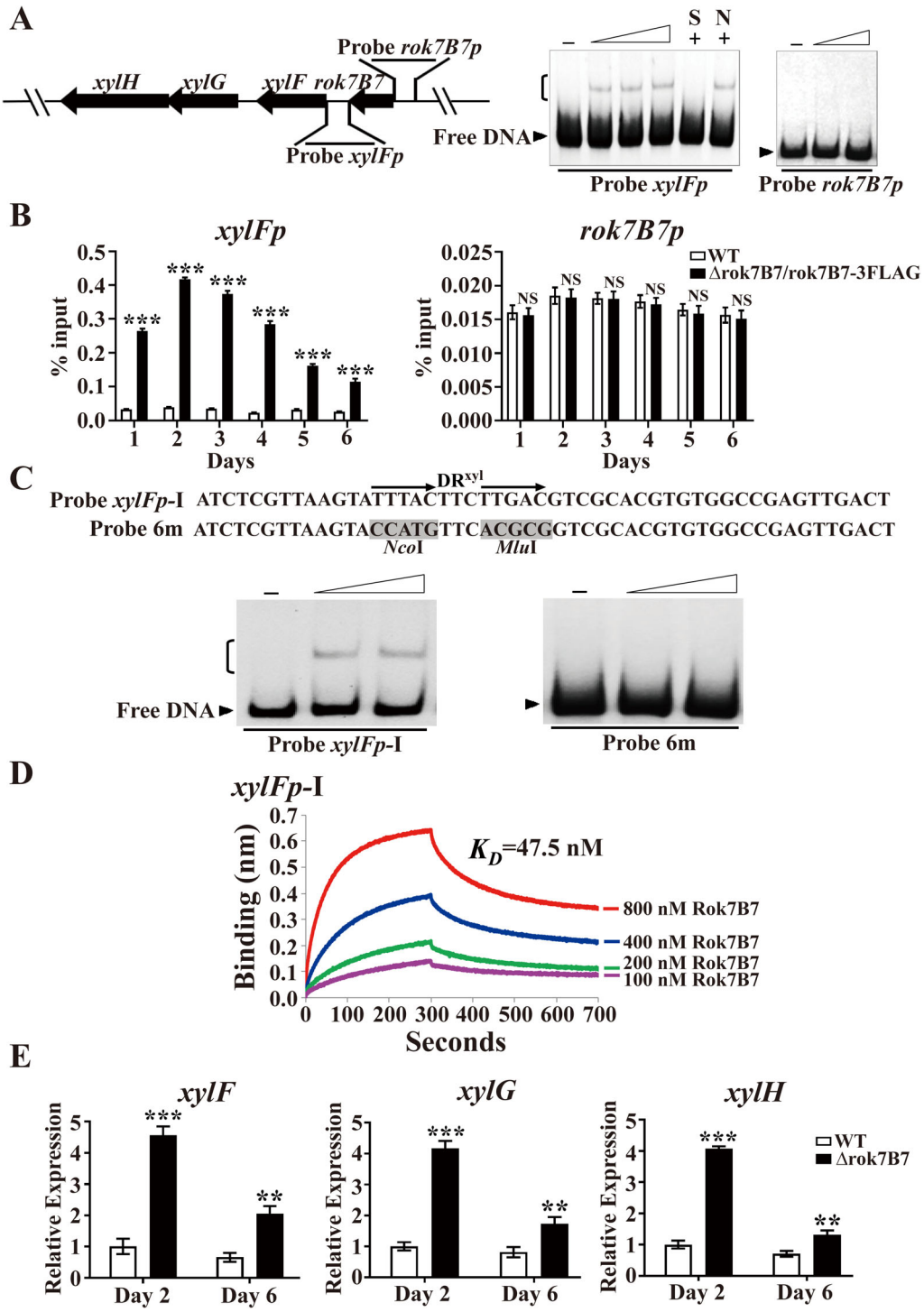

Fig. 7. Rok7B7 directly regulates *xylFGH* operon.
A. EMSAs of His_6-Rok7B7 using probes *xylFp* and *rok7B7p*. His_6-Rok7B7 concentrations for probe *xylFp*: 250, 500, and 750 nM; for probe *rok7B7p*: 500 and 750 nM. Lane notations (–, +, N, S) as in Fig. 4D.
B. ChIP-qPCR assays of Rok7B7 binding to *xylFp* and *rok7B7p*. Notations as in Fig. 4E.
C. EMSAs using 50-bp WT probe *xylFp*-I and its mutated probe 6 m. Direct repeats in probe *xylFp*-I were replaced with *Nco*I and *Mlu*I sites to produce mutated probe 6 m. Lanes 2 and 3 contained 500 and 750 nM His_6-Rok7B7.
D. BLI analysis of His_6-Rok7B7 binding to probe *xylFp*-I.
E. qRT-PCR analysis of *xylF*, *xylG*, and *xylH* in WT and Δrok7B7 grown in FM-I. Panels B, E: error bars: SD from triplicate experiments; NS, not significant; $^{**}P < 0.01$; $^{***}P < 0.001$ for comparison with WT (*t*-test). [Color figure can be viewed at wileyonlinelibrary.com]

repressor of *xylA* and *xylB* (Swiatek *et al*., 2013; Noguchi *et al*., 2018). Gene numbers for *xylABR* in *S. avermitilis* are *sav_7182* (*xylA*), *sav_7181* (*xylB1*), and *sav_7180* (*xylR*). *xylB1* is transcribed divergently from *xylA*, and convergently with *xylR* (Supporting Information Fig. S6A). However, binding of Rok7B7 to probe *xylRp* or *xylA_xylB1* (containing bidirectional promoters) was not observed (Supporting Information Fig. S6B).

Impact of rok7B7 deletion on xylose and glucose uptake

To investigate the effects of xylose and glucose on expression of *xylFGH*, transcription of *xylF* was analysed by qRT-PCR using RNAs isolated from WT or ΔrokB7 grown in liquid MM with xylose, glucose or xylose/glucose mixture as carbon sources. In WT, *xylF* transcription was enhanced by xylose within 12 h, but was strongly repressed in the presence of glucose and xylose/glucose (Fig. 8A), indicating that the *xylFGH* operon is subject to CCR. In ΔrokB7, *xylF* transcription was greatly increased under all conditions (Fig. 8A), consistent with repression of *xylFGH* by Rok7B7. Notably, glucose had no effect on *xylF* transcription in ΔrokB7, indicating that the repressing effect of glucose on *xylFGH* is mediated by Rok7B7. Xylose induced *xylF* transcription in ΔrokB7, suggesting that *xylFGH* operon is induced by xylose in both Rok7B7-dependent and -independent manners.

In a study of co-uptake of xylose and glucose by WT and ΔrokB7 in liquid MM cultures containing xylose and glucose, WT consumed 33% of glucose but only 4% of xylose during 72 h culture (Fig. 8B). In contrast, ΔrokB7 consumed glucose and xylose simultaneously, and eventually consumed 25% of glucose and 38% of xylose. Total sugars consumption was 63% for ΔrokB7 and 37% for WT; i.e., co-uptake efficiency of xylose and glucose was greatly improved by *rok7B7* deletion.

Xylose and glucose act as ligands of Rok7B7

To test whether xylose and glucose can act as ligands, EMSAs were performed to check the effect of the sugars on the affinity of Rok7B7 for *xylFp*. DNA-binding ability of Rok7B7 was impaired in the presence of xylose, but enhanced in the presence of glucose in a concentration-dependent manner (Fig. 8C). These findings were supported by BLI assays using probe *xylFp*-I (Fig. 8D), which showed that xylose and glucose serve as Rok7B7 ligands, but play opposite roles in modulating DNA-binding ability of Rok7B7. These findings, in combination with those from transcription analysis (Figs. 7E and 8A), allowed us to formulate a model of control of xylose uptake by Rok7B7 in response to xylose and glucose. Xylose acts as an inducer and, in the absence of glucose, releases Rok7B7 from *xylFp*, resulting in increased *xylFGH* expression for xylose uptake. In contrast, in the presence of a preferred carbon source as glucose, the affinity of Rok7B7 for its target site is enhanced.

To investigate whether the Rok7B7 orthologs from model strains *S. coelicolor* and *S. venezuelae* had similar binding affinities, the proteins were expressed as His_6-tagged proteins in *E. coli* and purified, and EMSAs were performed on the promoter region of *xylFsco* and *xylFsven*. This showed that also the Rok7B7 proteins of *S. coelicolor* and *S. venezuelae* bound to their respective *xylFGH* promoters (Supporting Information Fig. S7). DNA-binding affinity of the two proteins was inhibited by xylose, but enhanced by glucose (Supporting Information Fig. S7). These findings suggest wide conservation of the *cis-trans* relationships for Rok7B7 with the *xylFGH* operon and its control by glucose CCR in *Streptomyces* species.

Prediction and verification of new Rok7B7 target genes

Understanding of the broader roles of Rok7B7 in *S. avermitilis* requires identification of additional Rok7B7 target genes. Analysis of the 13-bp direct repeat sequences in the three Rok7B7-binding promoter regions mentioned above (*aveA1p*, *olmRIp*, *xylFp*) using WebLogo programme (http://weblogo.berkeley.edu) revealed a consensus sequence 5′-TTKAMKHSTTSAV-3′ (K = T/G; M = A/C; H = A/C/T; S = C/G; V = A/C/G) (Fig. 9A). Scanning of the *S. avermitilis* genome by PREDetector (Hiard *et al*., 2007) with the 13-bp consensus Rok7B7-binding sequence identified 275 putative Rok7B7 target genes (cut-off score ≥ 7) (Supporting Information Table S1). Of these, 82 were unknown or unclassified, and the remaining 193 were assigned to 17 groups on the basis of biological function as defined by the KEGG pathway database for *S. avermitilis*. Accuracy of the bioinformatic prediction was tested by selecting 23 well-annotated putative targets involved in primary metabolism, secondary metabolism, or development for EMSA confirmation.

Interestingly, one of the putative Rok7B7 target genes, *sav_2657*, encodes glucose transporter GlcP (van Wezel *et al*., 2005). While the gene was annotated as *araE* (for a putative L-arabinose permease) by the Genome Project of *S. avermitilis* (http://avermitilis.ls.kitasato-u.ac.jp), the gene product is identical to glucose permease GlcP in *S. coelicolor* (van Wezel *et al*., 2005). Rok7B7 bound well to probe *sav_2657p* (Fig. 9B). *sav_2657* transcription was significantly higher after 2 and 6 days for ΔrokB7 grown in FM-I than for WT, indicating that Rok7B7 acts as a repressor of this gene (Fig. 9C). Analysis of WT and ΔrokB7 grown in liquid MM containing

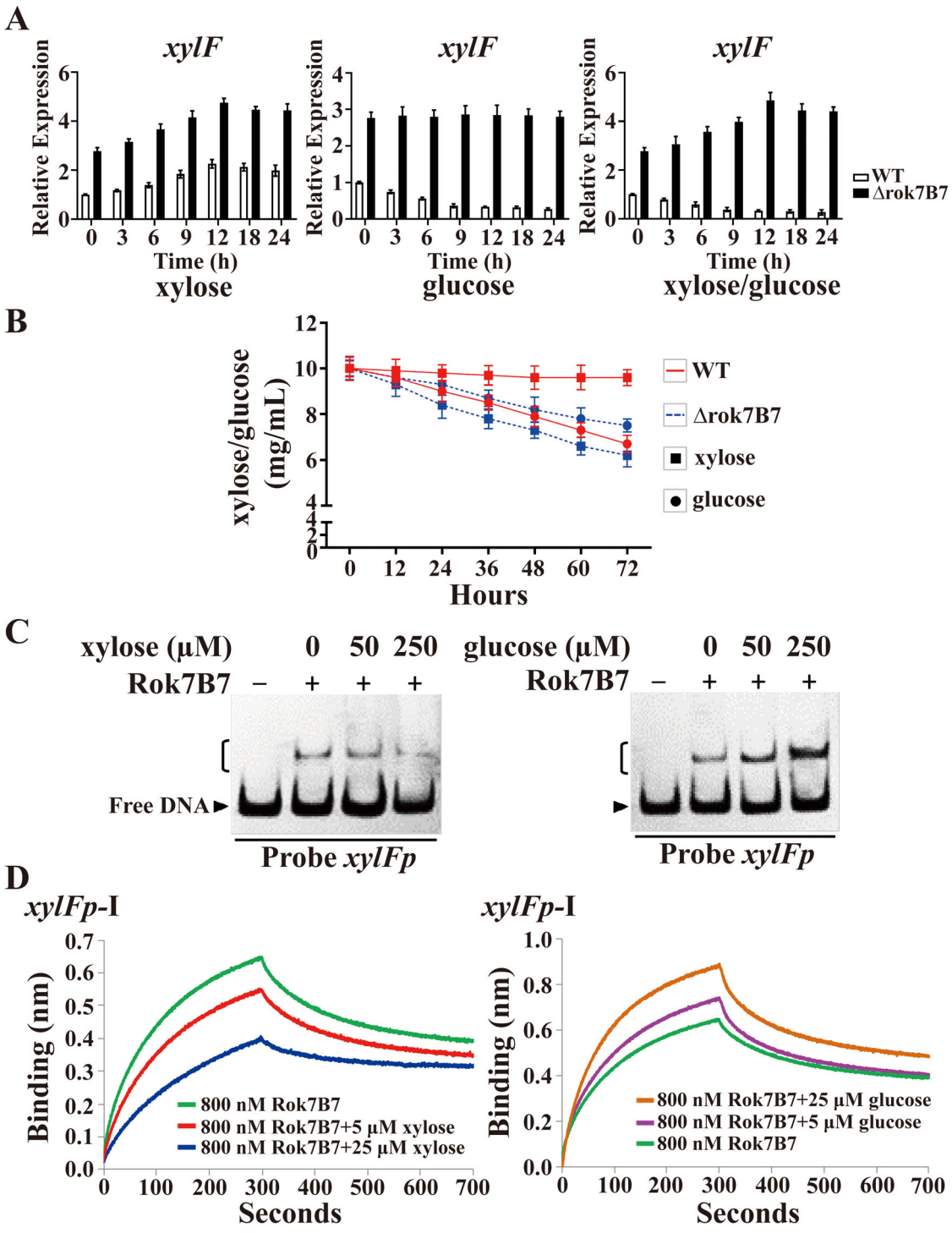

Fig. 8. Effects of xylose and glucose on DNA-binding activity of Rok7B7 to *xylFp*.
A. qRT-PCR analysis of *xylF* in WT and Δrok7B7 grown in MM containing xylose, glucose, or xylose/glucose combination. Cells were grown in MM containing mannitol (2 mg mL^{-1}) for 60 h, followed by addition of various sugars (each 10 mg mL^{-1}). *xylF* transcription level in WT before sugar addition (0 h) was defined as 1.
B. Consumption of glucose and xylose by WT and Δrok7B7 grown in MM containing xylose/glucose mixture (10 mg mL^{-1}). Error bars (panels A, B): SD from triplicate experiments.
C. EMSAs of His_6-Rok7B7 (500 nM) with xylose and glucose at indicated concentrations.
D. BLI analysis of His_6-Rok7B7 (800 nM) with xylose and glucose. [Color figure can be viewed at wileyonlinelibrary.com]

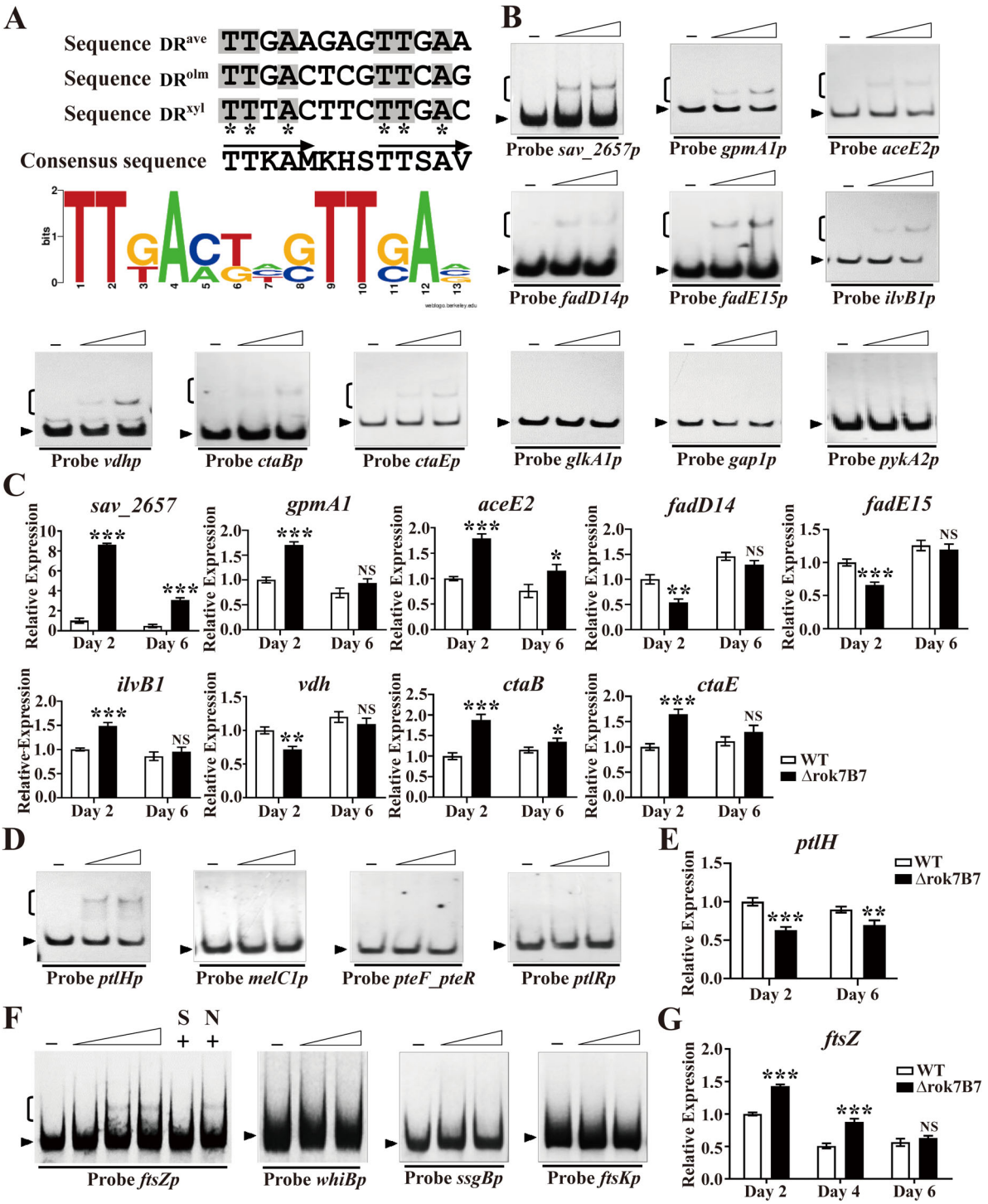

Fig. 9. Identification of new Rok7B7 targets.
A. Analysis of consensus Rok7B7-binding sequence by WebLogo programme. Arrows: conserved 5-bp direct repeats. Asterisks: consensus bases.
B. EMSAs of His_6-Rok7B7 with promoter regions of 12 predicted target genes associated with primary metabolism. Lanes 2 and 3 contained 500 and 750 nM His_6-Rok7B7.
C. qRT-PCR analysis of *sav_2657*, *gpmA1*, *aceE2*, *fadD14*, *fadE15*, *ilvB1*, *vdh*, *ctaB*, and *ctaE* in WT and Δrok7B7 grown in FM-I.
D. EMSAs of His_6-Rok7B7 with promoter regions of five predicted target genes associated with secondary metabolism.
E. qRT-PCR analysis of *ptlH* in WT and Δrok7B7 grown in FM-I.
F. EMSAs of His_6-Rok7B7 with four predicted target promoters associated with development. His_6-Rok7B7 concentrations for probe *ftsZp*: 250, 500, and 750 nM; for other promoter probes: 500 and 750 nM.
G. qRT-PCR analysis of *ftsZ* in WT and Δrok7B7 grown on YMS plates. Panels C, E, G: error bars: SD from triplicate experiments; NS, not significant; $*P < 0.05$; $**P < 0.01$; $***P < 0.001$ for comparison with WT (*t*-test). [Color figure can be viewed at wileyonlinelibrary.com]

arabinose, glucose, or arabinose/glucose mixture showed that *sav_2657* transcription was strongly induced by glucose, but unaffected by arabinose (Supporting Information Fig. S8). *sav_2657* transcription level was also notably increased by *rok7B7* deletion in each of the above three culture conditions. These findings suggest that Rok7B7 affects glucose uptake by directly repressing the gene *sav_2657* for the glucose permease GlcP.

EMSAs were performed on 11 additional putative Rok7B7 target genes associated with primary metabolism: *glkA1*, *gap1*, *gpmA1*, *pykA2*, *aceE2*, *fadD14*, *fadE15*, *ilvB1*, *vdh*, *ctaB*, and *ctaE* (Supporting Information Table S1). Rok7B7 bound directly to promoter regions of *gpmA1*, *aceE2*, *fadD14*, *fadE15*, *ilvB1*, *vdh*, *ctaB*, and *ctaE*, but not to those of *glkA1*, *gap1*, or *pykA2* (Fig. 9B). qRT-PCR analysis revealed that transcription levels of *gpmA1*, *aceE2*, *ilvB1*, *ctaB*, and *ctaE* were higher in Δrok7B7 than in WT, whereas those of *fadD14*, *fadE15*, and *vdh* were lower in Δrok7B7 (Fig. 9C). These findings demonstrate that Rok7B7 plays a pleiotropic role and displays dual repressor/activator function in primary metabolism.

Several putative Rok7B7 targets associated with secondary metabolism were also selected for EMSA evaluation: *melC1* involved in melanin biosynthesis; *pteF* and *pteR* in filipin biosynthesis (Vicente *et al*., 2014); *ptlR* and *ptlH* in biosynthesis of unknown terpene metabolite (Supporting Information Table S1). Rok7B7 bound only to probe *ptlHp*, but not to *melC1p*, *pteF-pteR* (bidirectional), or *ptlRp* (Fig. 9D). *ptlH* transcription level was reduced in Δrok7B7 (Fig. 9E), indicating that Rok7B7 acts as an activator of this newly identified target related to secondary metabolism.

In addition, several key genes involved in the onset of sporulation-specific cell division were included in the list of putative Rok7B7 targets, namely *whiB* (*sav_5042*) for the sporulatin protein WhiB (Bush *et al*., 2016), *ftsZ* (*sav_6124*) for the tubulin ortholog FtsZ that forms the cell division scaffold (Willemse *et al*., 2011; Schwedock *et al*., 1997), *ssgB* (*sav_4604*) for SsgB that recruits FtsZ to septum sites and thus activates sporulation-specific cell division (Willemse *et al*., 2011; Keijser *et al*., 2003), and *ftsK* (*sav_2510*) for FtsK that is required for chromosome segregation during cell division (Dedrick *et al*., 2009). Rok7B7 bound only to *ftsZp*, while it failed to bind to the other targets (Fig. 9F). qRT-PCR analysis of *ftsZ* transcription level using RNAs extracted from WT and Δrok7B7 grown on YMS plates for 2 (aerial growth), 4 (middle stage of sporulation), or 6 days (spore maturation) showed that the level was upregulated in Δrok7B7 on days 2 and 4 (Fig. 9G), consistent with the earlier developmental phenotype of Δrok7B7. These findings indicate that Rok7B7 negatively regulates development by directly repressing *ftsZ*.

Discussion

ROK-family regulator Rok7B7 was shown to play a functional role in *S. coelicolor* (Swiatek *et al*., 2013); however, until now little was known regarding its regulatory targets. We examined the molecular mechanism underlying Rok7B7 function in *S. avermitilis* and demonstrated that it functions in this species as an essential global regulator of development, antibiotic production, carbon uptake, and other primary metabolic processes through control of related target genes. Our findings provide an excellent basis for future studies of ROK-family regulators in *Streptomyces* species, and for construction of antibiotic-overproducing strains. We also revealed that Rok7B7 and its orthologs participate in glucose-mediated CCR of xylose uptake through direct regulation of xylose transport operon *xylFGH*, and DNA-binding activity of Rok7B7 on *xylFp* is modulated by glucose and xylose. Interestingly, several previous studies have shown that *Streptomyces* CCR is mediated through specific transcriptional regulators (Walter and Schrempf, 1996; Ni and Westpheling, 1997; Nguyen *et al*., 1997; Hindle and Smith, 1994; van Wezel *et al*., 1997), e.g., amylase and chitinase genes in *S. lividans* are regulated by a LacI/GalR-family regulator, Reg 1, which is involved in glucose repression (Nguyen *et al*., 1997); GylR (Hindle and Smith, 1994) and MalR (van Wezel *et al*., 1997), which control glycerol and maltose uptake in *S. coelicolor*, respectively, are required for both substrate induction and CCR. However, the detailed relationship of these regulators and Rok7B7 with GlkA is still unclear and requires further investigations.

Rok7B7 plays a differential role in regulation of avermectin and oligomycin A production, which are mediated respectively by structural genes and CSR gene. It also regulates the expression of the BGC directing the biosynthesis of an unknown terpene metabolite via activation of the expression of the structural gene *ptlH*. These findings demonstrate the pleiotropic and diverse role of Rok7B7 in the regulation of the expression of BGC. In many cases, pleiotropic/global regulators directly control CSR genes involved in antibiotic biosynthesis. However, there is increasing evidence that certain regulators, including *S. roseosporus* AtrA (Mao *et al*., 2015), *S. chattanoogensis* WhiG (Liu *et al*., 2015), *S. coelicolor* AfsQ1 (Chen *et al*., 2016), *S. avermitilis* SAV_742 (Sun *et al*., 2016), and Rok7B7 (present study) directly control specific antibiotic structural genes. Such direct regulatory mechanism of antibiotic biosynthesis may be universal in streptomycetes and facilitate rapid, precise regulation of antibiotic biosynthesis in response to various signals.

Concerning the control of xylose uptake, Rok7B7 acts as a direct repressor of *xylFGH* but not of another *xyl* gene locus, *xylABR*, consistent with the observation that

rok7B7 deletion in *S. coelicolor* had no effect on *xylABR* expression (Swiatek *et al*., 2013). XylR repressed *xylA* and *xylB* (Swiatek *et al*., 2013; Noguchi *et al*., 2018), and addition of xylose derepressed *xylA* expression in *S. avermitilis* (Noguchi *et al*., 2018), but the relationship between XylR and *xylFGH* was not previously investigated. In the present study, the expression of the *xylFGH* operon completely escaped glucose repression in ΔrokB7, but xylose still induced transcription of these genes, suggesting that *xylFGH* is controlled by other regulator(s). XylR is the most likely candidate, thus, its regulatory role on *xylFGH* remains to be more fully elucidated. In regard to glucose uptake, *S. coelicolor* contains two GlcP-encoding genes (*glcP1*, *glcP2*), and *glcP1* plays a major role in glucose transport (van Wezel *et al*., 2005). In *S. avermitilis*, *sav_2657* is the only gene homologous to *glcP1* and *glcP2*. Expression of *sav_2657*, as a Rok7B7 target, was strongly induced by glucose, but unaffected by arabinose, and *sav_2657* transcription level was strongly upregulated in ΔrokB7, consistent with the enhanced glucose uptake in this mutant. Thus, *sav_2657* evidently encodes a glucose permease involved in glucose transport, rather than an arabinose permease as annotated in the Genome Project of *S. avermitilis*.

Glucose and xylose are the major sugar components of lignocellulose, which is present in plant cell walls and has the potential to be developed as a renewable resource for microbial production of biofuels and other value-added bioproducts (Liguori *et al*., 2016). *Streptomyces* species produce enzymes used for lignocellulosic biomass hydrolysis (Pennacchio *et al*., 2018) and therefore can potentially be engineered to produce antibiotics or other useful products from lignocellulose hydrolysates. Efficient conversion of lignocellulosic materials requires simultaneous uptake of the two sugars. A common problem is that the presence of glucose inhibits xylose uptake by CCR. *rok7B7* deletion in *S. avermitilis* and *S. coelicolor* (Swiatek *et al*., 2013) enhanced both xylose and glucose uptake, and xylose uptake was not inhibited by glucose in ΔrokB7 mutant of *S. avermitilis*. *rok7B7* orthologous genes are widespread among *Streptomyces* species, and *rok7B7* deletion strategy therefore has great potential to improve co-uptake efficiency of glucose and xylose derived from lignocellulosic biomass and efficiency of fermentation process in streptomycetes.

Besides *sav_2657*, we identified eight new Rok7B7 targets involved in primary metabolism; *i.e*., genes involved in glycolysis (*gpmA1*, *aceE2*), fatty acid degradation (*fadD14*, *fadE15*), valine and isoleucine biosynthesis (*ilvB1*), valine degradation (*vdh*), and oxidative phosphorylation (*ctaB*, *ctaE*). These genes are closely associated with antibiotic biosynthesis. Glycolysis yields energy and acetyl-CoA, which become available for avermectin and oligomycin A biosynthesis. Fatty acid degradation provides acetyl-CoA precursor for biosynthesis of these two antibiotics. Starter units for avermectin biosynthesis are derived from valine and isoleucine (Ikeda and Omura, 1997). Thus, *ilvB1* and *vdh* are involved in providing starter units for avermectin biosynthesis. Oxidative phosphorylation is the main energy source for aerobic *Streptomyces*. Altered expression of *ctaB* and *ctaE* may thus affect energy supply for antibiotic biosynthesis. Rok7B7 represses *gpmA1*, *aceE2*, *ilvB1*, *ctaB*, and *ctaE*, but activates *fadD14*, *fadE15*, and *vdh*. Yield data obtained for avermectins and oligomycin A in ΔrokB7 therefore reflect a combined effect of altered expression of these primary metabolic genes. Avermectins and oligomycin A require common extender units for synthesis of polyketide chain (Omura *et al*., 2001); increase or decrease of antibiotic yields in ΔrokB7 may therefore be due in part to precursor competition between these two biosynthetic pathways.

We observed a negative regulatory role of Rok7B7 in *S. avermitilis* development, and identified the central cell division gene *ftsZ* as a Rok7B7 target. During sporulation, FtsZ is recruited to the septum site by SsgB to form a ladder of 50–100 Z rings in each sporogenic hypha to direct synthesis of sporulation septa (Willemse *et al*., 2011). In the mutant ΔrokB7, enhanced *ftsZ* expression contributed to earlier spore formation. However, possible contributions by other development-related Rok7B7 target genes to ΔrokB7 phenotype cannot be ruled out; further studies are needed to address this point.

A proposed schematic model of the Rok7B7-mediated regulatory network involved in primary metabolism (including xylose and glucose uptake), secondary metabolism, and development in *S. avermitilis* is shown in Fig. 10. The coordinated roles of Rok7B7 in these essential physiological processes are achieved through its regulatory effects on target genes. The promoter regions of several putative targets (*glkA1*, *gap1*, *pykA2, melC1*, *pteF, pteR*, *ptlR, whiB*, *ssgB*, *ftsK*) listed in the Supporting Information Table S1 were not bound by Rok7B7 *in vitro*. While we cannot explain this yet, it is tempting to suggest the presence of different classes of binding sites, as was previously observed for DasR (Swiatek-Polatynska *et al*., 2015). Another possibility is that such binding requires a specific ligand or an additional protein that contributes to its binding. The complex roles of Rok7B7 in streptomycetes will be progressively elucidated as we identify additional target genes and molecular processes.

Experimental procedures

Strains, plasmids, and growth conditions

Strains and plasmids used or constructed in this study are summarized in the Supporting Information Table S2,

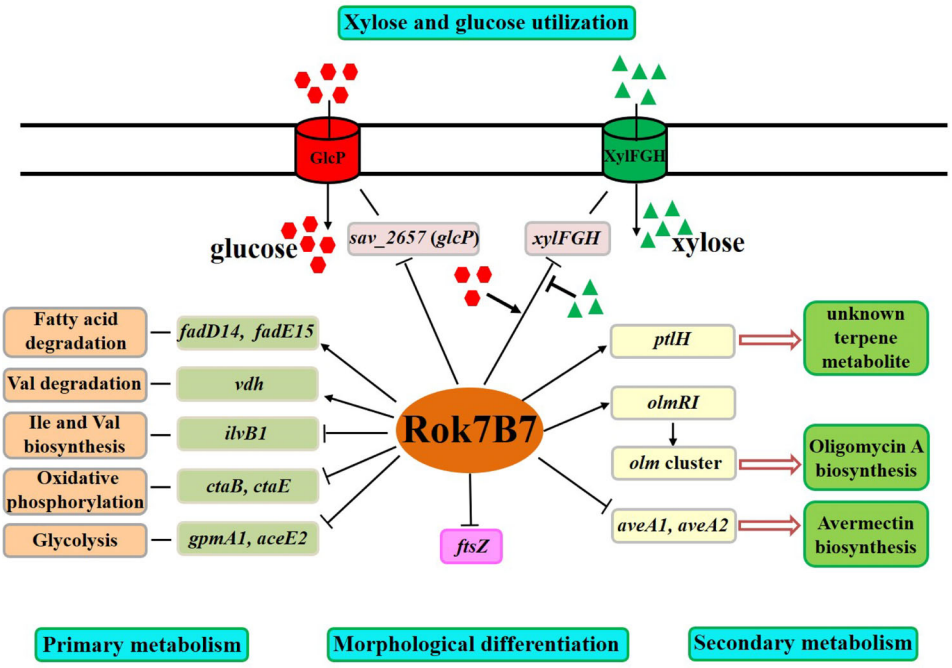

Fig. 10. Proposed schematic model of Rok7B7-mediated regulatory network in *S. avermitilis*. Bars: repression. Solid arrows: activation. Hollow arrows: production of secondary metabolites. Solid lines: involvement in primary metabolism. Triangles: xylose. Hexagons: glucose. [Color figure can be viewed at wileyonlinelibrary.com]

and primers are listed in the Supporting Information Table S3. Growth conditions for *E. coli* and *S. avermitilis* were described previously (Jiang *et al*., 2011). YMS (Ikeda *et al*., 1988) agar was used for phenotypic characterization of *S. avermitilis* mutants. Insoluble fermentation medium FM-I (Jiang *et al*., 2011) was used for avermectin and oligomycin A production, and soluble fermentation medium FM-II (Jiang *et al*., 2011) was used for quantitative analysis of *S. avermitilis* growth. Liquid MM (Kieser *et al*., 2000) supplemented with 10 mg mL^{-1} (1% w/v) of various carbon sources was used for analysis of carbon uptake.

Construction of S. avermitilis *mutants*

For in-frame gene deletion of *rok7B7*, a 418-bp 5′ flanking region and a 379-bp 3′ flanking region were amplified from WT genome with respective primer pairs LXR1A/LXR1B and LXR2A/LXR2B. The two fragments were digested, respectively, with *Bam*HI/*Xba*I and *Xba*I/*Eco*RI and then ligated into *Bam*HI/*Eco*RI-digested pKC1139 (Bierman *et al*., 1992), generating *rok7B7* deletion vector pDrok7B7, which was transformed into WT protoplasts. *rok7B7* deletion mutant Δrok7B7 was screened as described previously (Yang *et al*., 2015), confirmed by PCR with primers LXR5A/LXR5B (flanking the exchange regions) and LXR6A/LXR6B (located within the deletion region) (Supporting Information Fig. S2) and subjected to DNA sequencing. To delete *rok7B7* in industrial strain 63#, vector pDrok7B7 was transformed into 63# protoplasts. The mutant, termed Δrok7B7/63#, was isolated by selection of Δrok7B7 and confirmed by PCR with the same primers.

For complementation of Δrok7B7, a 1565-bp DNA fragment carrying *rok7B7* ORF and its promoter was amplified with primer pair LXR7A/LXR7B. The PCR product was cut out with *Xba*I/*Eco*RI and inserted into pSET152 (Bierman *et al*., 1992) to obtain *rok7B7*-complemented vector pSET152-rok7B7, which was then introduced into Δrok7B7 to obtain complemented strain Crok7B7.

For *rok7B7* overexpression, a 1249-bp DNA fragment containing *rok7B7* ORF was amplified with primers LXR4A/LXR4B, and ligated simultaneously with the 188-bp *ermE*p* fragment from pJL117 (Li *et al*., 2010) into pKC1139 to produce *rok7B7*-overexpressing vector pKC-erm-rok7B7, which was then introduced into WT to generate *rok7B7* overexpression strain Orok7B7.

To express 3 × FLAG-tagged Rok7B7 in *S. avermitilis*, *rok7B7* gene carrying its native promoter was amplified with primers LXR61A/LXR61B, and 3 × FLAG fragment was amplified from plasmid pIJ10500 (Pullan *et al*., 2011) with primers LXR60A/LXR60B. The resulting 1608-bp *rok7B7* and 100-bp FLAG fragments were ligated into pSET152 to generate pSET152-rok7B7-3FLAG, which was then transformed into Δrok7B7 to obtain recombinant strain Δrok7B7/rok7B7-3FLAG for expression of C-terminally 3 × FLAG-tagged Rok7B7.

Scanning electron microscopy

Streptomyces avermitilis WT and Δrok7B7 strains were inoculated onto YMS plates and incubated at 28°C for

2 or 4 days. Specimens were prepared and then observed by SEM as described previously (Sun *et al*., 2016).

Fermentation and analysis of antibiotics

Fermentation of *S. avermitilis* strains and quantitative analysis of avermectin and oligomycin A yield by HPLC were performed as described previously (Luo *et al*., 2014).

Determination of sugar content

Sugar content in fermentation broth was measured by HPLC. Fermentation broth (1 ml) was centrifuged at 13 000 × *g* for 15 min. The supernatant was filtered through nylon microporous (pore size 0.22 μm) membrane and applied to an HPLC system with ZORBAX Carbohydrate Analysis Column (5 μm; 4.6 × 250 mm; Agilent; USA) and refractive index detector RID-20A (Shimadzu; Japan). Glucose, xylose, maltose, and mannitol were separated with acetonitrile/water (80:20, v/v) at flow rate 1.0 ml min^{-1} and identified using respective standards.

qRT-PCR analysis

Total RNAs were extracted at various time points from *S. avermitilis* cultures grown in liquid FM-I, in MM containing various sugars, or on YMS plates, using TRIzol reagent (Tiangen; China). Reverse transcription and subsequent real-time PCR assays were performed as described previously (Luo *et al*., 2014). Transcription levels of tested genes were determined by qRT-PCR using respective primers, with housekeeping gene 16S *rRNA* as internal control to normalize samples. Each experiment was performed in triplicate.

Heterologous expression and purification of His_6-tagged Rok7B7 protein

For heterologous expression of *S. avermitilis* Rok7B7 in *E. coli*, the 1263-bp *rok7B7* coding region was amplified by PCR from genomic DNA of ATCC31267 using primer pair LXR3A/LXR3B. The PCR fragment was cut out with *Bam*HI/*Eco*RI and cloned into pET-28a (+), generating expression vector pET28-rok7B7, which was verified by sequencing. 1256-bp *rok7B7sco* gene was similarly amplified using primer pair LXR62A/LXR62B from genomic DNA of *S. coelicolor* M145, and 1267-bp *rok7B7sven* gene was amplified using primer pair LXR63A/LXR63B from genomic DNA of *S. venezuelae* ISP5230. The two PCR fragments were ligated into pET-28a (+) to obtain pET28-rok7B7sco and pET28-rok7B7sven, respectively. The three *rok7B7* expression vectors were transformed separately into *E. coli* Rosetta (DE3), and expression of N-terminal His_6-tagged Rok7B7 recombinant protein was induced by addition of 0.2 mM IPTG, followed by incubation for 3 h at 37°C. Cells were harvested, resuspended in lysis buffer (Guo *et al*., 2018), sonicated on ice, and centrifuged. Soluble recombinant protein from supernatant was purified using a Ni-NTA column (Bio-works; Sweden), and fractions eluted with 500 mM imidazole were dialyzed against binding buffer for EMSAs or HBS-EP buffer for BLI assays to eliminate imidazole. Protein concentration was determined by Bradford assay, and purified recombinant protein was stored at −80°C.

EMSAs

EMSAs were performed as described previously (Sun *et al*., 2016). Promoter probes containing putative Rok7B7-binding sequences were generated by PCR using corresponding primers, and 3′-terminally labelled with nonradioactive digoxigenin-1-ddUTP. In binding reactions (20 μl), 0.3 nM labelled probe was incubated with 1 μg poly [d(I-C)] and various amounts of His_6-Rok7B7 at 25°C for 30 min. Specificity of Rok7B7/probe interaction was confirmed by adding ∼300-fold excess of unlabeled *hrdBp* (nonspecific probe) or each specific probe to the reaction system.

For EMSAs with sugars, glucose or xylose was dissolved in deionized water and added to the reaction system at various final concentrations.

Western blotting

Western blotting was performed as described previously (Zhu *et al*., 2016). Total protein of Δrok7B7/rok7B7-3FLAG was prepared from mycelia grown in FM-I for various durations. Anti-FLAG M2 mouse antibody (mAb) (Sigma; USA) was used at ratio 1:3300.

ChIP-qPCR

Mycelia of *S. avermitilis* WT and Δrok7B7/rok7B7-3FLAG cultured in soluble FM-II for various times were collected, and processed as described previously (Yan *et al*., 2019). One millilitre input sample (2 mg protein/mL) was used for each immunoprecipitation, and 10 μl was kept as input DNA. The ChIP reaction was performed with 1 μl anti-FLAG mAb, and the immunoprecipitated DNA was quantified by real-time PCR using primer pairs listed in the Supporting Information Table S3. The WT strain was used as negative control. ChIP-qPCR data were normalized by the ratio of ChIP sample to input DNAand expressed as a percentage of input DNA. The relative values of protein enrichment were calculated

using the comparative Ct method: ΔCt (ChIP) = Ct (ChIP)-(Ct (Input)-6.644); Input% = $2^{-\Delta Ct\ (ChIP)} \times 100\%$. Each experiment was independently performed at least three times.

5′ RACE

Transcriptional start sites (TSSs) of *aveA1* and *olmRI* were determined by 5′ RACE using 5′/3′ RACE kit (Roche; USA). Total RNA (2 μg) extracted from 48-h culture of *S. avermitilis* WT grown in FM-I was used for reverse transcription with gene-specific primer sp1-aveA1 or sp1-olmRI (20 pmol). The obtained cDNAs were purified and treated with terminal transferase (TaKaRa; China) for addition of 3′ oligo(dA) tails. The tailed cDNA was PCR-amplified with oligo(dT) anchor primer and specific nested primer sp2-aveA1 or sp2-olmRI to yield a single specific band. The resulting PCR product was purified for sequencing, and TSS was mapped as the first base following oligo(dT) sequence.

BLI assay

BLI assay was performed using an Octet RED96 system (FortéBio; USA) to assess molecular interactions of Rok7B7 with its binding sequences. 5′ biotin-labelled 50-bp DNA fragments containing Rok7B7-binding sites were obtained by annealing primers listed in the Supporting Information Table S3. The reaction mixtures (each 200 μl) contained 300 nM biotin-labelled DNA probes and various concentrations of purified His_6-Rok7B7 in HBS-EP buffer [10 mM HEPES, 15 mM NaCl, 3 mM EDTA, 0.005% (v/v) Tween 20%, and 0.1% (w/v) BSA (pH 7.4)]. The assay procedure consisted of five steps: baseline, loading, washing, association, and dissociation. All steps were performed at 25°C in a 96-well plate containing 200 μl reaction mixture and a streptavidin (SA) biosensor probe in each well. Blank tests, for purpose of baseline balance, were performed using HBS-EP buffer instead of His_6-Rok7B7 in association step. Data were processed using software programme Octet Analysis 21 CFR, Part 11 (V. 9.0).

To analyse effects of ligands on binding of Rok7B7 to its target sequences, glucose or xylose was added to the reaction system at indicated concentrations.

Acknowledgements

This study was supported by the National Key Research and Development Program of China (Grant No. 2017YFD0201207) and the National Natural Science Foundation of China (Grant No. 31872629). The authors are grateful to Dr. S. Anderson for English editing of the manuscript.

References

Bekiesch, P., Forchhammer, K., and Apel, A.K. (2016) Characterization of DNA binding sites of RokB, a ROK-family regulator from *Streptomyces coelicolor* reveals the RokB regulon. *PLoS One* **11**: e0153249.

Bierman, M., Logan, R., O'Brien, K., Seno, E.T., Rao, R.N., and Schoner, B.E. (1992) Plasmid cloning vectors for the conjugal transfer of DNA from *Escherichia coli* to *Streptomyces* spp. *Gene* **116**: 43–49.

Burg, R.W., Miller, B.M., Baker, E.E., Birnbaum, J., Currie, S.A., Hartman, R., *et al*. (1979) Avermectins, new family of potent anthelmintic agents: producing organism and fermentation. *Antimicrob Agents Chemother* **15**: 361–367.

Bush, M.J., Chandra, G., Bibb, M.J., Findlay, K.C., and Buttner, M.J. (2016) Genome-wide chromatin immunoprecipitation sequencing analysis shows that WhiB is a transcription factor that cocontrols its regulon with WhiA to initiate developmental cell division in *Streptomyces*. *mBio* **7**: e00523–e00516.

Chen, S., Zheng, G., Zhu, H., He, H., Chen, L., Zhang, W., *et al*. (2016) Roles of two-component system AfsQ1/Q2 in regulating biosynthesis of the yellow-pigmented coelimycin P2 in *Streptomyces coelicolor*. *FEMS Microbiol Lett* **363**: fnw160.

Chen, Y., Wendt-Pienkowski, E., and Shen, B. (2008) Identification and utility of FdmR1 as a *Streptomyces* antibiotic regulatory protein activator for fredericamycin production in *Streptomyces griseus* ATCC 49344 and heterologous hosts. *J Bacteriol* **190**: 5587–5596.

Chng, C., Lum, A.M., Vroom, J.A., and Kao, C.M. (2008) A key developmental regulator controls the synthesis of the antibiotic erythromycin in *Saccharopolyspora erythraea*. *Proc Natl Acad Sci U S A* **105**: 11346–11351.

Dedrick, R.M., Wildschutte, H., and McCormick, J.R. (2009) Genetic interactions of *smc*, *ftsK*, and *parB* genes in *Streptomyces coelicolor* and their developmental genome segregation phenotypes. *J Bacteriol* **191**: 320–332.

Dubeau, M.P., Poulin-Laprade, D., Ghinet, M.G., and Brzezinski, R. (2011) Properties of CsnR, the transcriptional repressor of the chitosanase gene, *csnA*, of *Streptomyces lividans*. *J Bacteriol* **193**: 2441–2450.

Egerton, J.R., Ostlind, D.A., Blair, L.S., Eary, C.H., Suhayda, D., Cifelli, S., *et al*. (1979) Avermectins, new family of potent anthelmintic agents: efficacy of the B1a component. *Antimicrob Agents Chemother* **15**: 372–378.

Flardh, K., and Buttner, M.J. (2009) *Streptomyces* morphogenetics: dissecting differentiation in a filamentous bacterium. *Nat Rev Microbiol* **7**: 36–49.

Guo, J., Zhang, X., Lu, X., Liu, W., Chen, Z., Li, J., *et al*. (2018) SAV4189, a MarR-family regulator in *Streptomyces avermitilis*, activates avermectin biosynthesis. *Front Microbiol* **9**: 1358.

Guo, J., Zhao, J., Li, L., Chen, Z., Wen, Y., and Li, J. (2010) The pathway-specific regulator AveR from *Streptomyces avermitilis* positively regulates avermectin production while it negatively affects oligomycin biosynthesis. *Mol Genet Genomics* **283**: 123–133.

Hiard, S., Maree, R., Colson, S., Hoskisson, P.A., Titgemeyer, F., van Wezel, G.P., *et al*. (2007) PREDetector: a new tool to

identify regulatory elements in bacterial genomes. *Biochem Biophys Res Commun* **357**: 861–864.

Hindle, Z., and Smith, C.P. (1994) Substrate induction and catabolite repression of the *Streptomyces coelicolor* glycerol operon are mediated through the GylR protein. *Mol Microbiol* **12**: 737–745.

Ikeda, H., Kotaki, H., Tanaka, H., and Omura, S. (1988) Involvement of glucose catabolism in avermectin production by *Streptomyces avermitilis*. *Antimicrob Agents Chemother* **32**: 282–284.

Ikeda, H., Nonomiya, T., Usami, M., Ohta, T., and Omura, S. (1999) Organization of the biosynthetic gene cluster for the polyketide anthelmintic macrolide avermectin in *Streptomyces avermitilis*. *Proc Natl Acad Sci U S A* **96**: 9509–9514.

Ikeda, H., and Omura, S. (1997) Avermectin biosynthesis. *Chem Rev* **97**: 2591–2610.

Jiang, L., Liu, Y., Wang, P., Wen, Y., Song, Y., Chen, Z., and Li, J. (2011) Inactivation of the extracytoplasmic function sigma factor σ^6 stimulates avermectin production in *Streptomyces avermitilis*. *Biotechnol Lett* **33**: 1955–1961.

Kazanov, M.D., Li, X., Gelfand, M.S., Osterman, A.L., and Rodionov, D.A. (2013) Functional diversification of ROK-family transcriptional regulators of sugar catabolism in the *Thermotogae phylum*. *Nucleic Acids Res* **41**: 790–803.

Keijser, B.J., Noens, E.E., Kraal, B., Koerten, H.K., and van Wezel, G.P. (2003) The *Streptomyces coelicolor ssgB* gene is required for early stages of sporulation. *FEMS Microbiol Lett* **225**: 59–67.

Kieser, T., Bibb, M.J., Buttner, M.J., Chater, K.F., and Hopwood, D.A. (2000) *Practical Streptomyces Genetics*, Norwich, UK: The John Innes Foundation.

Kitani, S., Ikeda, H., Sakamoto, T., Noguchi, S., and Nihira, T. (2009) Characterization of a regulatory gene, *aveR*, for the biosynthesis of avermectin in *Streptomyces avermitilis*. *Appl Microbiol Biotechnol* **82**: 1089–1096.

Li, L., Guo, J., Wen, Y., Chen, Z., Song, Y., and Li, J. (2010) Overexpression of ribosome recycling factor causes increased production of avermectin in *Streptomyces avermitilis* strains. *J Ind Microbiol Biotechnol* **37**: 673–679.

Liguori, R., Ventorino, V., Pepe, O., and Faraco, V. (2016) Bioreactors for lignocellulose conversion into fermentable sugars for production of high added value products. *Appl Microbiol Biotechnol* **100**: 597–611.

Lin, X., Wen, Y., Li, M., Chen, Z., Guo, J., Song, Y., and Li, J. (2009) A new strain of *Streptomyces avermitilis* produces high yield of oligomycin A with potent anti-tumor activity on human cancer cell lines in vitro. *Appl Microbiol Biotechnol* **81**: 839–845.

Liu, S.P., Yu, P., Yuan, P.H., Zhou, Z.X., Bu, Q.T., Mao, X.M., and Li, Y.Q. (2015) Sigma factor WhiGch positively regulates natamycin production in *Streptomyces chattanoogensis* L10. *Appl Microbiol Biotechnol* **99**: 2715–2726.

Luo, S., Sun, D., Zhu, J., Chen, Z., Wen, Y., and Li, J. (2014) An extracytoplasmic function sigma factor, σ^{25}, differentially regulates avermectin and oligomycin biosynthesis in *Streptomyces avermitilis*. *Appl Microbiol Biotechnol* **98**: 7097–7112.

Mao, X.M., Luo, S., Zhou, R.C., Wang, F., Yu, P., Sun, N., *et al*. (2015) Transcriptional regulation of the daptomycin gene cluster in *Streptomyces roseosporus* by an autoregulator, AtrA. *J Biol Chem* **290**: 7992–8001.

Nguyen, J., Francou, F., Virolle, M.J., and Guerineau, M. (1997) Amylase and chitinase genes in *Streptomyces lividans* are regulated by *reg1*, a pleiotropic regulatory gene. *J Bacteriol* **179**: 6383–6390.

Ni, X., and Westpheling, J. (1997) Direct repeat sequences in the *Streptomyces* chitinase-63 promoter direct both glucose repression and chitin induction. *Proc Natl Acad Sci U S A* **94**: 13116–13121.

Noguchi, Y., Kashiwagi, N., Uzura, A., Ogino, C., Kondo, A., Ikeda, H., and Sota, M. (2018) Development of a strictly regulated xylose-induced expression system in *Streptomyces*. *Microb Cell Fact* **17**: 151.

Omura, S., Ikeda, H., Ishikawa, J., Hanamoto, A., Takahashi, C., Shinose, M., *et al*. (2001) Genome sequence of an industrial microorganism *Streptomyces avermitilis*: deducing the ability of producing secondary metabolites. *Proc Natl Acad Sci U S A* **98**: 12215–12220.

Pennacchio, A., Ventorino, V., Cimini, D., Pepe, O., Schiraldi, C., Inverso, M., and Faraco, V. (2018) Isolation of new cellulase and xylanase producing strains and application to lignocellulosic biomasses hydrolysis and succinic acid production. *Bioresour Technol* **259**: 325–333.

Pinna, L.A., Lorini, M., Moret, V., and Siliprandi, N. (1967) Effect of oligomycin and succinate on mitochondrial metabolism of adenine nucleotides. *Biochim Biophys Acta* **143**: 18–25.

Plumbridge, J. (2001) Regulation of PTS gene expression by the homologous transcriptional regulators, Mlc and NagC, in *Escherichia coli* (or how two similar repressors can behave differently). *J Mol Microbiol Biotechnol* **3**: 371–380.

Pullan, S.T., Chandra, G., Bibb, M.J., and Merrick, M. (2011) Genome-wide analysis of the role of GlnR in *Streptomyces venezuelae* provides new insights into global nitrogen regulation in actinomycetes. *BMC Genomics* **12**: 175.

Romero-Rodriguez, A., Robledo-Casados, I., and Sanchez, S. (2015) An overview on transcriptional regulators in *Streptomyces*. *Biochim Biophys Acta* **1849**: 1017–1039.

Romero-Rodriguez, A., Rocha, D., Ruiz-Villafan, B., Guzman-Trampe, S., Maldonado-Carmona, N., Vazquez-Hernandez, M., *et al*. (2017) Carbon catabolite regulation in *Streptomyces*: new insights and lessons learned. *World J Microbiol Biotechnol* **33**: 162.

Schwedock, J., McCormick, J.R., Angert, E.R., Nodwell, J. R., and Losick, R. (1997) Assembly of the cell division protein FtsZ into ladder-like structures in the aerial hyphae of *Streptomyces coelicolor*. *Mol Microbiol* **25**: 847–858.

Sun, D., Zhu, J., Chen, Z., Li, J., and Wen, Y. (2016) SAV742, a novel AraC-family regulator from *Streptomyces avermitilis*, controls avermectin biosynthesis, cell growth and development. *Sci Rep* **6**: 36915.

Swiatek, M.A., Gubbens, J., Bucca, G., Song, E., Yang, Y. H., Laing, E., *et al*. (2013) The ROK family regulator Rok7B7 pleiotropically affects xylose utilization, carbon catabolite repression, and antibiotic production in *Streptomyces coelicolor*. *J Bacteriol* **195**: 1236–1248.

Swiatek-Polatynska, M.A., Bucca, G., Laing, E., Gubbens, J., Titgemeyer, F., Smith, C.P., *et al*. (2015)

Genome-wide analysis of in vivo binding of the master regulator DasR in *Streptomyces coelicolor* identifies novel non-canonical targets. *PLoS One* **10**: e0122479.

Tanaka, A., Takano, Y., Ohnishi, Y., and Horinouchi, S. (2007) AfsR recruits RNA polymerase to the *afsS* promoter: a model for transcriptional activation by SARPs. *J Mol Biol* **369**: 322–333.

van Wezel, G.P., Mahr, K., Konig, M., Traag, B.A., Pimentel-Schmitt, E.F., Willimek, A., and Titgemeyer, F. (2005) GlcP constitutes the major glucose uptake system of *Streptomyces coelicolor* A3(2). *Mol Microbiol* **55**: 624–636.

van Wezel, G.P., and McDowall, K.J. (2011) The regulation of the secondary metabolism of *Streptomyces*: new links and experimental advances. *Nat Prod Rep* **28**: 1311–1333.

van Wezel, G.P., White, J., Young, P., Postma, P.W., and Bibb, M.J. (1997) Substrate induction and glucose repression of maltose utilization by *Streptomyces coelicolor* A3(2) is controlled by *malR*, a member of the LacI-GalR family of regulatory genes. *Mol Microbiol* **23**: 537–549.

Vicente, C.M., Santos-Aberturas, J., Payero, T.D., Barreales, E.G., de Pedro, A., and Aparicio, J.F. (2014) PAS-LuxR transcriptional control of filipin biosynthesis in *S. avermitilis*. *Appl Microbiol Biotechnol* **98**: 9311–9324.

Walter, S., and Schrempf, H. (1996) The synthesis of the *Streptomyces reticuli* cellulase (avicelase) is regulated by both activation and repression mechanisms. *Mol Gen Genet* **251**: 186–195.

Willemse, J., Borst, J.W., de Waal, E., Bisseling, T., and van Wezel, G.P. (2011) Positive control of cell division: FtsZ is recruited by SsgB during sporulation of *Streptomyces*. *Genes Dev* **25**: 89–99.

Yan, H., Lu, X., Sun, D., Zhuang, S., Chen, Q., Chen, Z., *et al*. (2019) BldD, a master developmental repressor, activates antibiotic production in two *Streptomyces* species. *Mol Microbiol* **113**, 123–142.

Yang, R., Liu, X., Wen, Y., Song, Y., Chen, Z., and Li, J. (2015) The PhoP transcription factor negatively regulates avermectin biosynthesis in *Streptomyces avermitilis*. *Appl Microbiol Biotechnol* **99**: 10547–10557.

Yin, S., Wang, W., Wang, X., Zhu, Y., Jia, X., Li, S., *et al*. (2015) Identification of a cluster-situated activator of oxytetracycline biosynthesis and manipulation of its expression for improved oxytetracycline production in *Streptomyces rimosus*. *Microb Cell Fact* **14**: 46.

Yu, Q., Bai, L.Q., Zhou, X.F., and Deng, Z.X. (2012) Inactivation of the positive LuxR-type oligomycin biosynthesis regulators OlmRI and OlmRII increases avermectin production in *Streptomyces avermitilis*. *Chin Sci Bull* **8**: 869–876.

Zhu, J., Sun, D., Liu, W., Chen, Z., Li, J., and Wen, Y. (2016) AvaR2, a pseudo gamma-butyrolactone receptor homologue from *Streptomyces avermitilis*, is a pleiotropic repressor of avermectin and avenolide biosynthesis and cell growth. *Mol Microbiol* **102**: 562–578.

Supporting Information

Additional Supporting Information may be found in the online version of this article at the publisher's web-site:

Appendix S1: Supporting information